https://doi.org/10.5194/egusphere-2026-275
Preprint. Discussion started: 16 February 2026

Particle flux dynamics amplify marine carbon cycle differences between climate states

Markus Adloff[1,2], Frerk Pöppelmeier[1,2], Ashley Dinauer[1,2], Charlotte Laufkötter[1,2], and Fortunat Joos[1,2]

[1]Climate and Environmental Physics, Physics Institute, University of Bern, Switzerland
[2]Oeschger Centre for Climate Change Research, University of Bern, Switzerland

Correspondence: Markus Adloff (markus.adloff@bristol.ac.uk)

Abstract.

The ocean represents the largest and most rapidly exchanging carbon reservoir on Earth's surface and the marine carbon cycle response to changing climate is a matter of continuous investigation. Here, we added dynamic environmental controls on the remineralization and dissolution rates of particulate organic matter, carbonate and silicate minerals (Dinauer et al., 2022) to the Earth system model Bern3D to explore feedbacks between biogenic particle fluxes and marine carbon cycling under different climate conditions. The new representation of marine particle dynamics improves the model's ability to capture the marine biogeochemical response to long-term cooling, almost doubles the sensitivity of global export production, and amplifies the change in marine carbon storage by a factor of about 1.5. In a model configuration where carbon exclusively cycles between the atmosphere and ocean, this corresponds to an additional atmospheric CO_2 drawdown or increase of approximately 20 ppm in response to a -9.1°C cooling or +6.8°C warming, respectively.

1 Introduction

The partitioning of carbon between the atmosphere and ocean is influenced by the cycling of organic and inorganic biogenic matter within the ocean, causing lower concentrations of dissolved inorganic carbon (DIC) and alkaliniy (ALK) at the surface ocean and lower atmospheric CO_2 compared to an ocean with absent biogenic matter cycling Volk and Hoffert (1985).

Dissolved carbon and macro- and micronutrients enter the marine ecosystem through uptake by autotrophic organisms in the surface ocean. The resulting organic matter is then cycled through the food chain and ends up in either dissolved (DOM) or particulate (POM) organic matter. The dissolved fraction is transported by the ocean circulation and is subjected to chemical degradations where temperature and redox conditions are conducive. Organic particles, which often form aggregates with inorganic particles like carbonates and biogenic opal, sink through the water column due to gravitational settling. The majority of POM is remineralized and transformed back into dissolved forms above the thermocline, such that nutrients are directly recycled for continued surface primary production. Yet, a small fraction of POM is not decomposed during the sinking and reaches the sea floor, entering marine sediments. Remineralization of sinking organic particles and dissolution of carbonate and opal below the well-mixed surface ocean layer transfer carbon, cations, ALK, and nutrients from the photic zone to the intermediate and deep ocean, which is largely balanced in steady-state by corresponding upward fluxes by physical transport

https://doi.org/10.5194/egusphere-2026-275
Preprint. Discussion started: 16 February 2026

(advection, convection, diffusion). These transfer fluxes by sinking particles and the circulation lead to vertical gradients in DIC, ALK, and nutrients, and are referred to as the biological soft tissue and carbonate pumps (Volk and Hoffert, 1985). This mechanism substantially influences the partitioning of carbon between the atmosphere and the ocean and is expected to change under past and future climate change (Matsumoto, 2007; Matsumoto et al., 2007; Kwon et al., 2009; Segschneider and Bendtsen, 2013; Roth et al., 2014).

The effectiveness of the soft tissue and carbonate pumps in maintaining low surface ocean carbon concentrations depends on the rates of particle (and DOM) production and export, particle concentration profiles, and circulation. The vertical attenuation profile of particles has been shown to be strongly influenced by temperature, oxygen concentrations (Bendtsen et al., 2002; Taucher et al., 2014; Laufkötter et al., 2017) and, in the case of carbonates, carbonate chemistry. The attenuation profile is furthermore dependent on the sinking speed of the particles, which depends on their mass, geometry, and extent of coagulation with other particles (Armstrong et al., 2001, 2009; Dinauer et al., 2022). The availability of limiting nutrients such as iron, phosphate, and silica exerts a strong control on production rates, and can change with shifting circulation patterns, attenuation rates, and climate and ocean state dependent sedimentary burial and terrigenic supply.

To capture these manifold processes, simulations of the ocean's future carbon cycle response to anthropogenic climate change relies on increasingly complex biogeochemical representations that are rarely validated for climate states other than the present, while Earth system models that are regularly employed to simulate past climate states still rely on simplified implementations of biogenic particle cycling (Hülse et al., 2017). This creates a barrier to assessing the role of changing biogenic particle dynamics in the long-term response of the ocean to climatic changes.

Proxy evidence and model simulations suggest that biologically-mediated marine carbon storage changes occurred in response to the orbitally-induced climatic changes of the last glacial cycles. Specifically, temperature-driven changes of the remineralization profile and a partial alleviation of iron limitation during glacial phases have a large potential to alter the biologically-mediated marine carbon storage over glacial-interglacial cycles (e.g. Buchanan et al., 2016; Galbraith and Skinner, 2020; Adloff et al., 2025). Some reconstructed changes in regional export production during the last glacial have also been attributed to changed availability of nitrogen and iron (Fe) (Martin, 1990; Deutsch et al., 2004). Yet, no model produces proxy-consistent marine carbon cycle changes without prescribing further changes in biogeochemistry, but require climate state-dependent parameter choices and forcings to represent pre-industrial and glacial carbon cycling (e.g. Galbraith and Skinner, 2020). This indicates that these models partly lack the dynamics that determine the response of the biological pump to climatic changes, reducing the model skill of simulating climatic states that differ from the pre-industrial.

Here, we test how the marine carbon cycle and atmospheric CO_2 are affected by dynamical particle cycling in different climate states by adopting the columnar explicit particle flux model MSPACMAM (Dinauer et al., 2022) as a fully integrated module in the intermediate complexity Earth system model Bern3D, alongside an updated Fe cycle. We evaluate the model performance against proxy evidence of marine carbon cycling in a glacial state and assess how the added processes alter the model's response to idealized warming.

The Bern3D model has been used to simulate carbon cycle dynamics in various scenarios of environmental change of the past and future, but only with globally-uniform, static particle attenuation profiles, relying on climate state-dependent

https://doi.org/10.5194/egusphere-2026-275
Preprint. Discussion started: 16 February 2026

parameter adjustments as a simplified representation of the climatic controls on export production and remineralization (e.g. Jeltsch-Thömmes et al., 2019) and a simple Fe cycle without a dynamic sedimentary Fe source (Parekh et al., 2004, 2008).

2 Methods

2.1 Bern3D

Bern3D is an Earth system model of intermediate complexity, including a 3D ocean, 2D atmosphere with energy-moisture balance, 3D icesheet, thermodynamic sea-ice, and a marine biogeochemistry module that is coupled to a dynamic sediment model. In the most recent model version v3.0 (Pöppelmeier et al., 2023) all components share a 68×46 irregular horizontal grid with higher resolution in the Atlantic, Southern Ocean and Eastern Equatorial Pacific. The ocean contains 40 logarithmically-scaled depth layers, and the upper 10 cm of marine sediments are divided into 10 uneven depth layers with higher resolution at the surface. The physical component of the ocean model is based on frictional geostrophy (Edwards et al., 1998; Müller et al., 2006) with parameterizations for spatially variable diapycnal diffusion (St. Laurent et al., 2002), isopycnal diffusion and transport by eddies (Griffies, 1998).

The marine biochemistry component contains 20 tracers and is described in detail in Parekh et al. (2008); Tschumi et al. (2008); Battaglia and Joos (2018b). Bern3D does not have an explicit tracer for organic biomass. Instead, all primary production and other ecosystem processes are parameterized implicitly by calculating the net phosphate incorporation into organic export production based on local light- and nutrient-limitations and temperature (Doney et al., 2006). The uptake of other biogeochemcial tracers is calculated based on fixed Redfield ratios. While the biological uptake and transformation processes are treated implicitly, the resulting organic export production is simulated explicitly within the model. In the previous model version, biogenic particle transfer from the ocean's surface to the ocean-sediment interface was approximated by using a power law to describe the remineralization of the export flux with depth below the euphotic zone (Martin 1987; $F(z) = F(z=0) \cdot (z/z_0)^{\alpha}$ with $\alpha = -0.83$ in oxic and -0.03 in suboxic waters) (Battaglia and Joos, 2018b). Biogenic carbonate and opal dissolve exponentially below the euphotic zone with globally uniform length scales. The Fe cycle was simplified by prescribing a constant sedimentary Fe source from continental shelves, uniform Fe-binding ligand concentrations and reversible scavenging by organic and carbonate particles (Parekh et al., 2004, 2008).

For the present study, we implemented an implicit version of the columnar dynamic particle flux model MSPACMAM (Dinauer et al., 2022) to add environmental controls to the remineralization and dissolution profiles of biogenic particles. Specifically, the remineralization of particulate organic matter (POM) is now sensitive to local temperature and O_2:

$$rPOM = k_{POM} \cdot e^{aE \cdot (T - T_{ref})} \cdot \frac{O_2}{O_2 + k_{O_2}} \quad (1)$$

k_{POM} being the remineralization rate constant, aE an exponent for temperature modification, T_{ref} a reference temperature for remineralization and k_{O_2} the half-saturation constant for O_2 uptake.

https://doi.org/10.5194/egusphere-2026-275
Preprint. Discussion started: 16 February 2026

The dissolution of carbonate is sensitive to the local saturation state Ω where $\Omega < 1$:

$$rCaCO_3 = Rres + k_{calc} \cdot SSA_{calc} \cdot (1-\Omega)^{n_{calc}} \quad (2)$$

differentiating between aragonite and calcite and with faster dissolution if $\Omega \leq 0.8$. k_{calc} represents the dissolution rate constant, SSA_{calc} the specific surface area of the particle and n_{calc} the reaction order for carbonate dissolution. We also followed Liang et al. (2023) in allowing carbonate dissolution in marine particles above the lysocline if organic matter remineralization occurs locally (indicated by the term $Rres$ in the equation above, see SI). Sinking speeds are calculated for the mix of organic, carbonate and opal particles exported from the euphotic zone based on the average density of the particle mix and the viscosity of the surrounding water:

$$w = (\sqrt{\frac{4}{3} \cdot 981 \cdot r^3 \cdot \rho_{seawater} \cdot (\rho_{particlemix} - \rho_{seawater}) + 9 \cdot \nu^2} - 3 \cdot \nu)/(\rho_{seawater} \cdot r) \quad (3)$$

r is the particle radius, $\rho_{seawater}$ and $\rho_{particlemix}$ are the densities of seawater and the particle mix, respectively, and ν is the viscosity.

As in Dinauer et al. (2022), we consider two particle size classes (small and large) with independent porosities, carbonate dissolution rates, and sinking speeds.

We provide further information on the particle flux scheme in the SI, and detailed derivations of the underlying relationships are provided in Dinauer et al. (2022).

In addition, we updated marine Fe cycling for a better representation of Fe limitation on export production. Specifically, we adopted the dynamic ligand and particle-specific scavenging parameterisations from Nickelsen et al. (2015), Dale et al. (2015) and Somes et al. (2021). Furthermore, we added authigenic Fe particle coagulation and scavenging following Tagliabue et al. (2023).

$$\frac{dFe}{dt} = inFe_{Hydrothermal} + inFe_{dust} + inFe_{sediment} - aPFe_{POM} - aPFe_{authigenic} - Fe_{scavenged} + Fe_{regenerated} \quad (4)$$

The new Fe budget is expressed in equation 4 and Fig. S1.1. dFe denotes the change in Fe concentration (free, colloidal, and ligand-bound). Besides Fe inputs from dust ($inFe_{dust}$, derived from the dust field already prescribed for other soluble tracers (Mahowald et al., 2006)), the model now considers inputs from hydrothermal vents ($inFe_{hydrothermal}$, based on Muglia et al. (2017)) and recycled Fe from the seafloor sediments ($inFe_{sediment}$, explained in more detail in SI). Uptake during export production in the euphotic zone $aPFe_{POM}$ (functionally unchanged compared to the previous model version), authigenic Fe particle formation ($aPFe_{authigenic}$, explained in more detail in SI) and scavenging ($Fe_scavenged$, also explained in SI) remove Fe (any, colloidal and free, respectively) from the ocean. Scavenged Fe and Fe taken up during export production is

https://doi.org/10.5194/egusphere-2026-275
Preprint. Discussion started: 16 February 2026

regenerated and released to the water column ($Fe_{regenerated}$) in proportion to the remineralization or dissolution rate of the respective particles.

The new particle flux and Fe schemes, as well as the tuning of the parameters for an equilibrium pre-industrial state are described in detail in supplementary text S1.

The tuned new model version, including the new modules and a set of standard parameter values, is labeled v3.1. For the experiments in this manuscript, the sediment module and the ice sheet modules are not enabled.

2.2 Experiment design

To explore the effects of the new environmental controls on particle fluxes and the marine carbon cycle, we performed simulations with the ocean-atmosphere modules of Bern3D in three setups (Tab. 1). These include the old (*Martin*) and new (*Particle*) model versions. An intermediate version which includes dynamic particle fluxes but not the updates to the Fe scheme (*Particle_oldFe*) is used to isolate the effect of the new particle scheme from that of the Fe cycle updates.

We performed simulations under pre-industrial ('PI'), cooler ('cold'), and warmer ('warm') than present climate states with each model setup to explore the effects of the new environmental controls on particle fluxes and the marine carbon cycle. This yields in total 9 simulations (3 model setups $\times$ 3 climate states). For the three PI simulations, the model was spun up under preindustrial conditions for 10 kyr as a physical ocean-only system, followed by 15 kyr coupled to the dynamic atmospheric energy-moisture balance and 10 kyr with all biogeochemical tracers included to bring the atmosphere-ocean system close to equilibrium. Remaining drift in ocean tracers, including $\delta^{13}C$, are negligible. For the three cold simulations, a negative step change in radiative forcing of 8 W/m^2 was applied to the PI equilibrium state and the model was run for 10 kyr under this fixed radiative forcing. This yields a global cooling of $\approx$ 9°C, which is at the upper end of estimated global mean surface temperature differences between the Last Glacial Maximum (LGM) and the pre-industrial Earth system state (Tierney et al., 2020). Atmospheric CO_2 decreases from its PI value in response to the cooling but is in these sensitivity simulations not influencing radiative forcing and climate. The setup of the three warm simulations is the same as for the cold simulations but a positive step change in radiative forcing of 8 W/m^2 is applied. This forcing is similar to the effective radiative forcing of the abrupt 4×CO2 CMIP6 experiment (Smith et al., 2020; Poletti et al., 2024) and yields a warming of about 6.8 °C.

Table 1. The three model setups for the Bern3D model, in the configuration without the dynamic ocean sediment and ice sheet modules

Model setup	Particle fluxes		Fe update	
	Martin curve	MSPACMAM	no	yes
Martin	X		X	
Particle		X		X
Particle_oldFe		X	X	

https://doi.org/10.5194/egusphere-2026-275
Preprint. Discussion started: 16 February 2026

In each experiment, we explicitly trace preformed quantities (DIC, O_2, ALK, PO_4^{2-}). Preformed quantities are set equal to the respective total quantities at the surface and then get transported alongside all other tracers but are not affected by any biogeochemical processes in the ocean. The difference between total and preformed quantities in the ocean interior then gives the regenerated quantities.

In addition to this set of principle simulations, we ran a sensitivity experiment by including the marine sediment module (spun up for an additional 50 kyr) to test the difference between estimated and calculated sedimentary POC respiration on the sedimentary Fe source.

3 Results

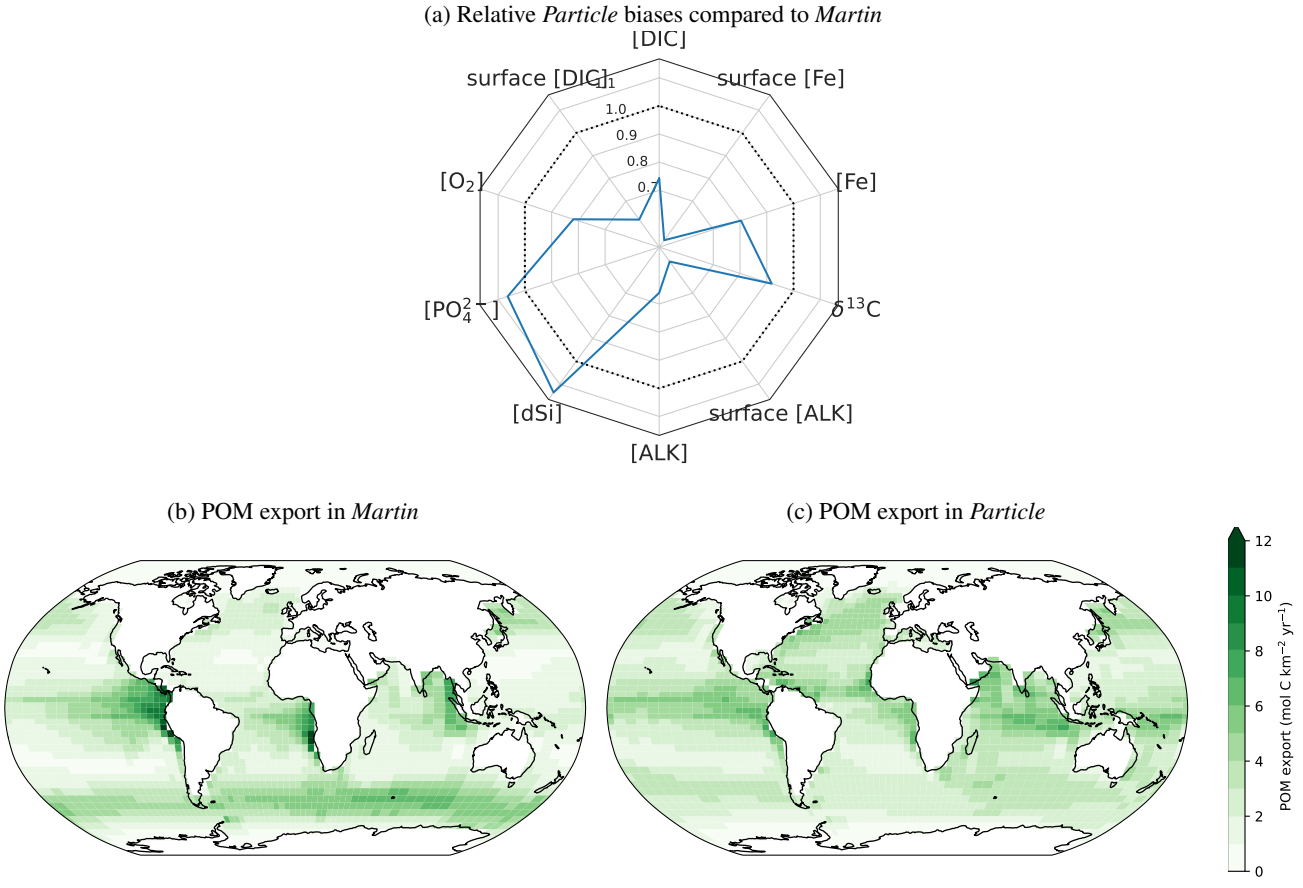

Figure 1. (a) shows the bias in tracer distributions compared to observational data (WOA 2018, GEOTRACES 2021 v2) in the tuned pre-industrial steady state of *Particle* (blue line) relative to that of *Martin*. The center point represents relative biases $\leq$0.5. A value of 1 in any given tracer indicates that the respective bias is as big as in *Martin*. Spatial patterns of annual mean POM export production in the tuned pre-industrial steady state are shown in (b) for *Martin* and (c) for *Particle*.

https://doi.org/10.5194/egusphere-2026-275
Preprint. Discussion started: 16 February 2026

With both set ups, *Martin* and *Particle*, the model is tuned to minimise biasses against observed biogeochemical tracer distributions in in the modern ocean (Parekh et al., 2008; Tschumi et al., 2008; Battaglia and Joos, 2018b, and SI). In *Particle*, biases in the simulated distribution of most biogeochemical tracers are reduced compared to *Martin* (Fig. 1, see SI for more details about the model tuning), suggesting that the additional processes contribute to the observed tracer distributions. This is especially true for Fe in the surface ocean, which are strongly reduced by the updated Fe dynamics. In consequence, *Particle* features increased Fe limitation on export production than *Martin*, especially in the Southern Ocean (SI, Fig. S1.7). The most consequential differences between the pre-industrial steady states are therefore substantially lower POM export production in the Southern Ocean in *Particle* than *Martin*, as well as higher export production in the North Atlantic and Indian Ocean due to nutrient re-distributions. Note that significant biases remain, partially due to too sluggish AABW and AAIW ventilation (Pöppelmeier et al., 2023).

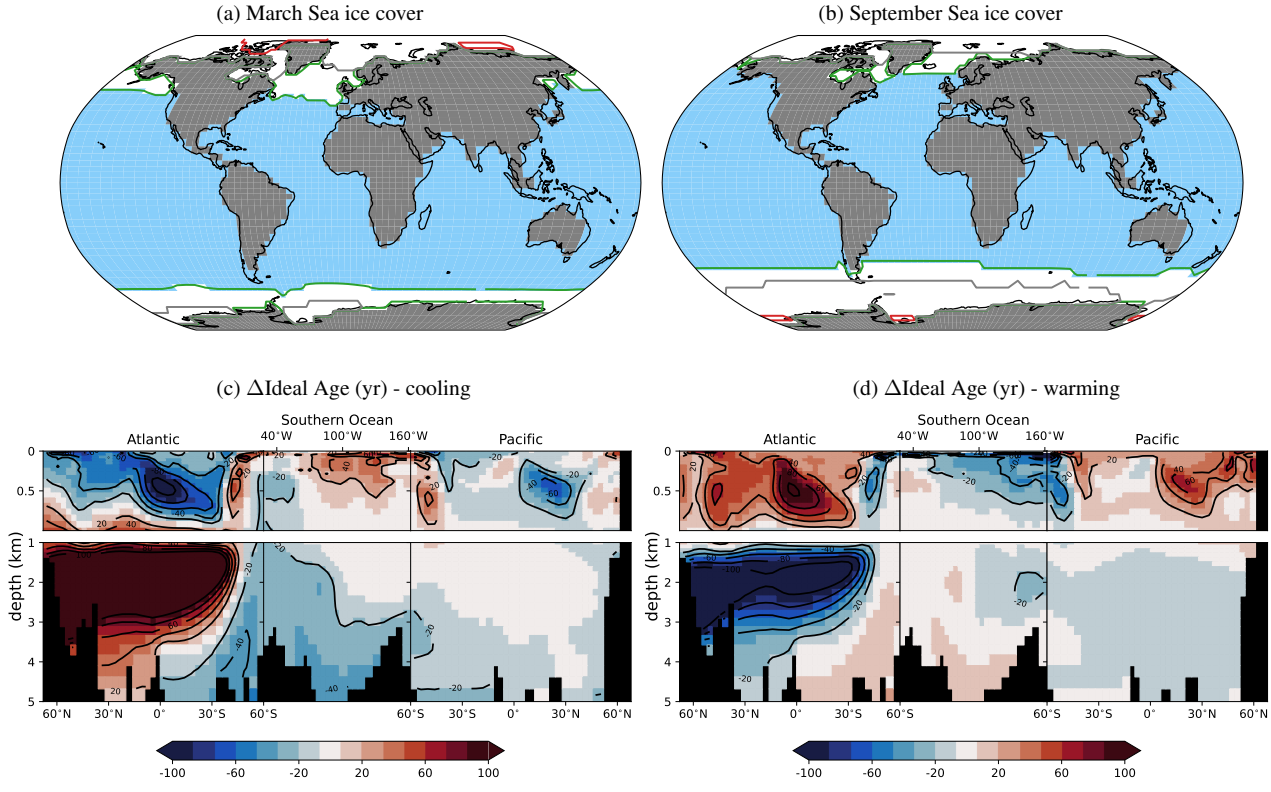

Figure 2. Sea ice cover (a-b) and changes of ideal age of the ocean's interior (c-d) in our cooling and warming simulations. Panels a-b show sea ice margins (>20% sea ice cover) in March and September, respectively, in the pre-industrial climate (gray lines) the cold climate state (green lines and area plotted in white) and the warm climate state (red lines, if any sea ice is simulated). Grid cells with less than 20% sea ice cover in every simulation are shown in blue. Panels c-d show changes of the ideal age tracer along a continuous transect through the Atlantic, Southern Ocean and Pacific. The ideal age tracer increases by 1 every model year and is re-set to zero at the surface.

https://doi.org/10.5194/egusphere-2026-275
Preprint. Discussion started: 16 February 2026

The physical response to the applied radiative forcings in the *cold* and *warm* simulations are the same regardless of model set up, since we disabled the climate feedback of carbon cycle changes. The 9.1 °C cooling due to the applied negative radiative forcing in our cold climate state simulations causes a substantial sea ice expansion in the polar oceans (by $36 \cdot 10^{12}$ km^2), AMOC weakening (a reduction of the maximum value of the overturning streamfunction between 30°N–60°N from 17.25 to 8 Sv) and an increase in the average ideal water mass age in the ocean of nearly 200 yr (Fig. 2a,c). Conversely, the applied positive radiative forcing in our warm climate state simulations reduces polar sea ice by $22 \cdot 10^{12}$ km^2 and strengthens AMOC by 5.5 Sv, reducing the water mass age in the deep North Atlantic (Fig. 2b,d). These climatic changes affect marine biogeochemical cycles in all simulations but the amplitude of these changes varies between our model setups.

Table 2. Global changes in atmospheric CO_2, marine carbon and oxygen storage and organic export production due to cooling (-9.1°C) and warming (+6.8°C) in the different model setups (all without dynamic terrestrial carbon storage, ice sheets, and sediments).

Model setup	ΔCO_2 (ppm)	$\Delta CO_2/\Delta T$ (ppm/K)	ΔDIC (mmol/m^3)	ΔDIC (Pg C)	ΔO_2 (mmol/m^3)	ΔExport (Pg C/yr)
Cooling						
Martin	-48	5.27	+6.1	-10.9	-9.9	-2.2
Particle_oldFe	-54	5.93	+7.5	-13.4	-7.0	-5.3
Particle	-66	7.25	+10.7	-19.2	-27.4	-4.8
Warming						
Martin	+49	7.21	-7.5	-17.9	-37.6	+2.4
Particle	+77	11.32	-9.3	-22.3	-23.5	+3.5

Including the dynamic particle flux model MSPACMAM into Bern3D amplifies climate-driven changes in marine carbon storage, especially when combined with the updated Fe cycle (Table 2). In the simplified Earth system setup employed here that only includes the two dynamic carbon stores of ocean and atmosphere, the elevated sensitivity to climate change of marine carbon storage translates directly into a stronger atmospheric CO_2 response (see also Fig. S2.1). Hence, in the warming and cooling experiments, the representation of particle dynamics amplifies the atmospheric CO_2 change due to climate change by up to 28 ppm. The added model complexity also strongly alters the magnitudes of POM export and marine O_2 concentration changes under climate change.

To better understand the processes behind the altered biogeochemical response due to particle dynamics, we first analyze how climate change affects marine carbon and O_2 dynamics under prescribed invariant remineralization profiles (simulations *Martin*), and then examine how dynamic particle fluxes alter the model behaviour. The processes by which the dynamic particle flux scheme affects the marine carbon cycle response to cooling and warming are similar but their effect is of opposite sign. Hence, we first describe the processes in detail for the cooling scenario, and then summarize the effects of the same processes in the warming scenario.

3.1 Response to cooling in simulations *Martin*

https://doi.org/10.5194/egusphere-2026-275
Preprint. Discussion started: 16 February 2026

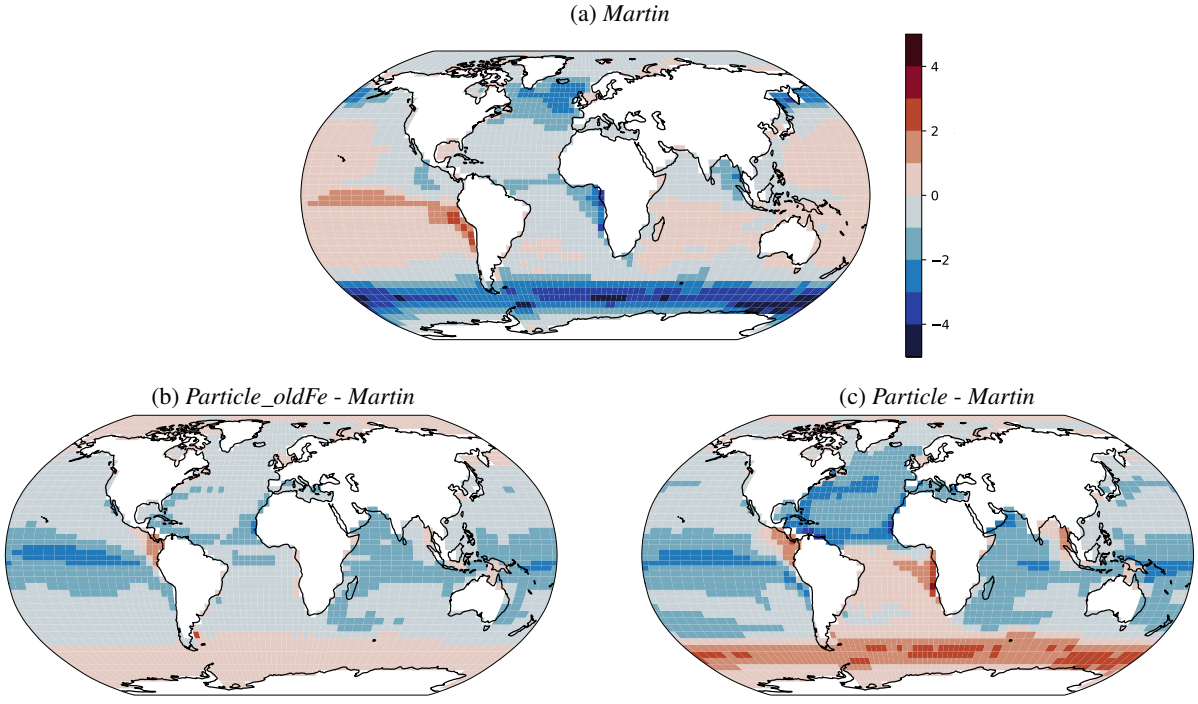

Figure 3. Changes of annual mean POM export due to the applied cooling in *Martin* ($Martin_{cold}$ - $Martin_{PI}$) (a) and the differences to this response in simulations *Particle_oldFe* (b) and *Particle* (c).

Export production, which is temperature, nutrients, and light-dependent, is strongly reduced by the cooling and sea ice advances in the polar and subpolar oceans (Fig. 3a). Upwelling of nutrient-rich deep water near western continental margins decreases (Fig. S2.2), and is shifted southward in the Pacific, leading to reduced export production in the Bay of Bengal, South Atlantic, and Eastern Equatorial Pacific. In contrast, export production is slightly increased due to elevated nutrient delivery to the coastal Pacific off South America in simulation $Martin_{cold}$ compared to $Martin_{PI}$.

Overall, the globally colder temperatures lead to an increase of the mean DIC concentration by 6.2 mmol/m^3, equivalent to 100 Pg of additional C storage in the ocean, and reduces the mean O_2 concentration by 10 mmol/m^3 in the setup *Martin* with the static Martin curve remineralization (Tab 2).

https://doi.org/10.5194/egusphere-2026-275
Preprint. Discussion started: 16 February 2026

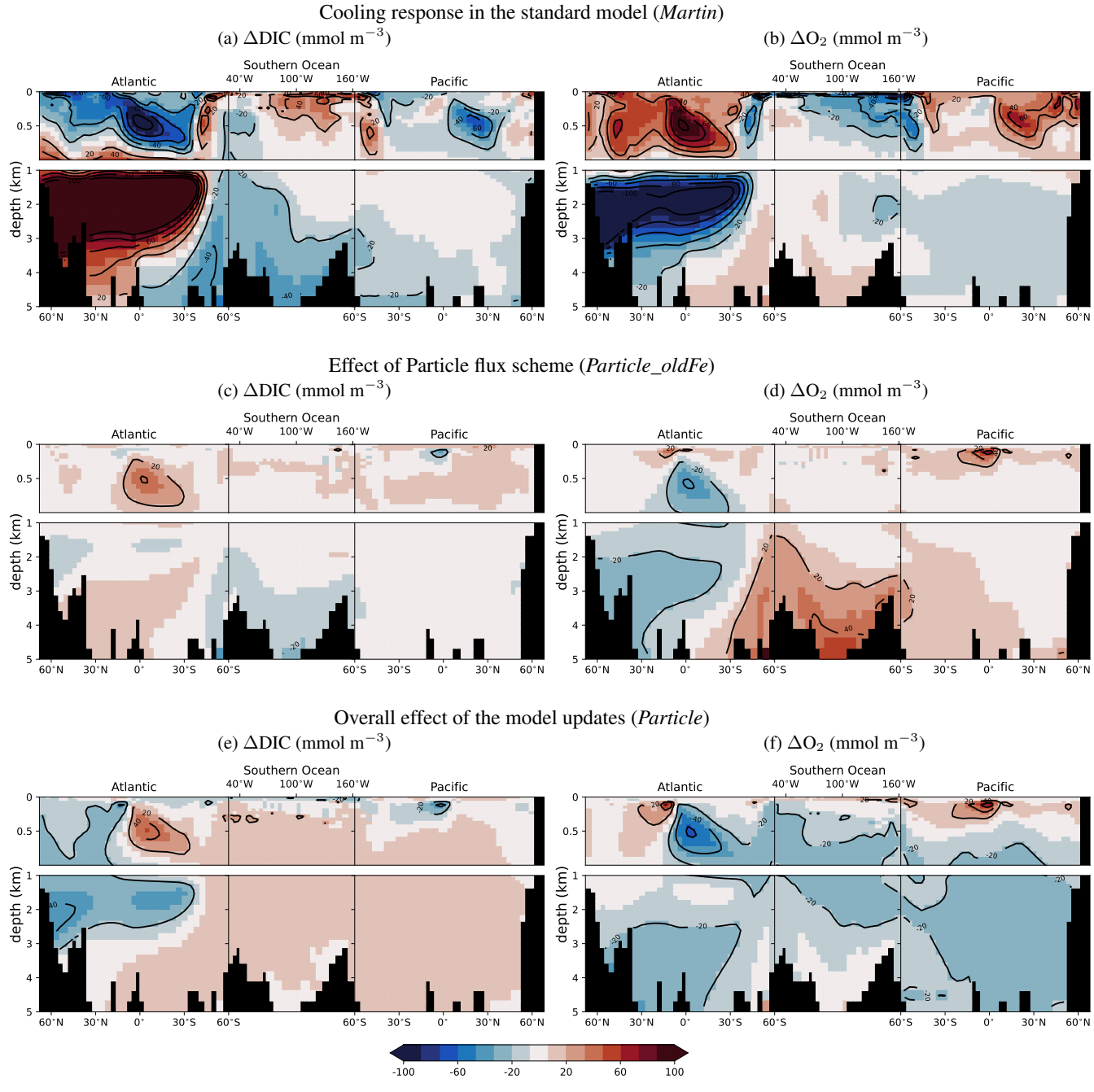

Figure 4. The isolated effects of adding the particle flux scheme (the difference between $Particle\_oldFe_{cold}$ minus $Particle\_oldFe_{PI}$ and $Martin_{cold}$ minus $Martin_{PI}$, upper row) and the updated Fe cycle (the difference between $Particle_{cold}$ minus $Particle_{PI}$ and $Particle\_oldFe_{cold}$ minus $Particle\_oldFe_{PI}$, middle row) on changes of DIC and O_2 concentration profiles due to the applied cooling, as well as the overall effect (difference between $Particle_{cold}$ minus $Particle_{PI}$ and $Martin_{cold}$ minus $Martin_{PI}$, bottom row)

https://doi.org/10.5194/egusphere-2026-275
Preprint. Discussion started: 16 February 2026

190 These changes are primarily the result of changes in the North Atlantic (Fig. 4a,b), where the simulated shoaling of AMOC leads to the largest biogeochemical changes, with reduced (preformed) DIC in the upper water column due to the strong weakening of deep convection in the North Atlantic and associated reduced northward transport of DIC in the upper water column and a large DIC increase at depth (both preformed and regenerated, Fig. S2.5) and deep O_2 decline. In the upper water column of the Southern Ocean and Pacifc, DIC and O_2 concentration changes are mostly the result of changes in sea ice and
195 export production. Cooling of the surface ocean increases the saturation concentration of O_2 and CO_2 but expansion of sea ice limits the exposure of surface waters in subpolar and polar oceans to the atmosphere. C and O_2 solubilities increase but are overcompensated by increased DIC and O_2 saturation disequilibria in the Southern Ocean (Fig. S2.5) that get transported into the deep ocean (Cliff et al., 2021; Liu et al., 2024), resulting in a small O_2 concentration decrease in the deep Pacific ocean in response to cooling.

200 ### 3.1.1 Cooling scenario with the dynamic particle scheme

The responses of the physical components of the Earth system are independent of the biogeochemical setup in our simulations, as the radiative forcing is prescribed independent of simulated atmospheric CO_2 changes. However, the biogeochemical cycling of nutrients, carbon, and oxygen within the water column is substantially altered by including particle dynamics and updating the Fe cycle.

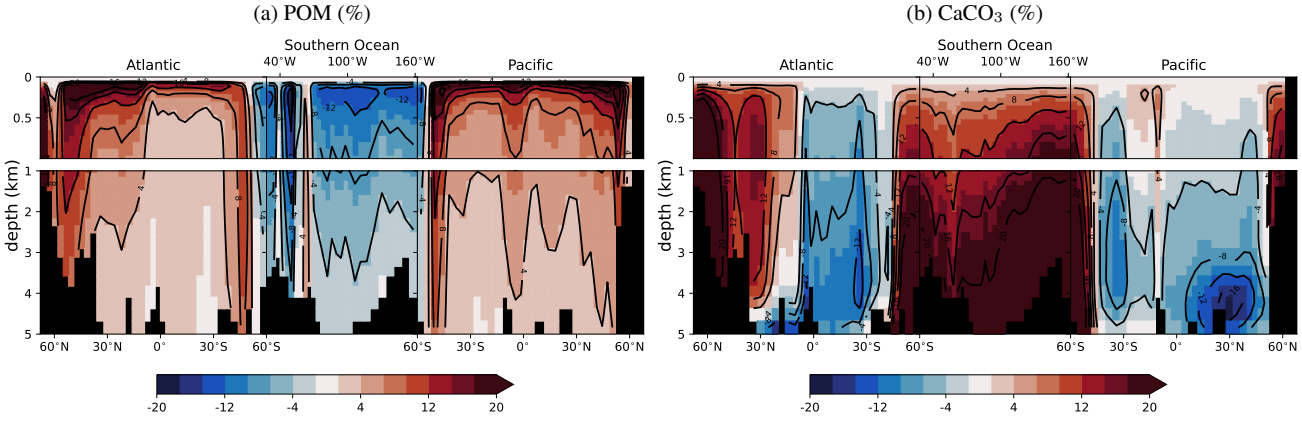

Figure 5. Changes in transfer efficiency due to cooling with the dynamic particle scheme (simulation $Particle_{cold}$ minus $Particle_{PI}$). Transfer efficiency at a given depth is defined as the percentage of export flux at 100 m that reaches that depth, shown are changes in absolute percentage points.

205 With the new parameterization of particle dynamics, the percentage of the export flux that reaches the deep North Atlantic increases compared to PI conditions in the cooling experiment($Particle_{cold}$ minus $Particle_{PI}$) for all particle types that we consider here (Fig. 5) while overall export production decreases. Cooling and oxygen loss in the North Atlantic increase POM preservation because the remineralization rate is explicitly dependent on temperature and O_2 concentration. Carbonate

https://doi.org/10.5194/egusphere-2026-275
Preprint. Discussion started: 16 February 2026

saturation decreases in simulation *Particle*$_{cold}$ relative to *Particle*$_{PI}$, particularly in the North Atlantic (Fig. S2.3), but the water remains saturated down to below 2500 m depth. In saturated waters, carbonate dissolution on marine particles only occurs due to in-situ organic carbon remineralization (Liang et al., 2023). Thus, reduced POM remineralization directly entails reduced $CaCO_3$ dissolution.

In the rest of the non-polar oceans, the changes of POM and $CaCO_3$ transfer efficiencies are largely of opposite sign. Increases in POM transfer efficiency are generally concentrated in the upper part of the water column while for $CaCO_3$ the largest declines are simulated in the deep. Increased POM preservation in the upper ocean is predominantly driven by the cooling itself which reduces remineralization rates in the upper water column. The higher ratio of POM to $CaCO_3$ in the sinking particles lowers the sinking speed, which prolongs the time during which the particles are subjected to the local remineralization and dissolution rates. Hence, the percentage of POM that reaches the deep sea sediments changes little overall, while $CaCO_3$ is less stable in the water column.

Also in the Southern Ocean, cooling slows the remineralization rate of POM, but the loss of ballasting due to reduced opal production dominates and decreases the sinking speed of particles. Moving more slowly through the water column, their residence time increases and a larger fraction of the exported POM is remineralised and less POM reaches the deep Southern Ocean. In other words, the transfer efficiency of POM is reduced in the Southern Ocean and a larger fraction of POM is remineralized in the upper ocean. Since POM export itself is reduced due to the cooling, the overall amount of POM remineralized in the deep Southern Ocean is, in absolute terms, lower in the cold climate state than in PI. This reduces $CaCO_3$ dissolution rates. Further, the reduced $CaCO_3$ export results in more ALK being subducted, raising $CaCO_3$ saturation. These two effects result in increased particulate $CaCO_3$ preservation in the Southern Ocean in the simulations with cooling (*Particle*$_{cold}$) compared to the PI state (*Particle*$_{PI}$), although the absolute $CaCO_3$ flux is minimal.

These particle flux changes alter the response of the marine carbon cycle to cooling. The downward shift of respiration in the water column reduces nutrient recycling in the upper water column, reducing PO_4 concentrations in the surface ocean (Fig. S2.4) and thus export production throughout most of the ocean, except the upwelling zones where deep water, now more nutrient-enriched, is returned to the surface (Fig. 3b). This reduction of export production reduces the O_2 loss and DIC gain in the deep ocean except in the Atlantic, where amplified cooling increases POM preservation sufficiently to out-compete the effect of reduced export to cause a net increase of respiration in the deep (Fig. 4a,b). Across the shallow ocean, the temperature-driven reduction of remineralization rates increases O_2 concentrations (Fig. 4b).

Overall, the new biogeochemical setup (*Particle*) results in a larger marine DIC increase and O_2 loss in response to cooling, expressed throughout most of the ocean (Fig 4e,f) than in our simulation with Martin curve and the simple Fe cycle (*Martin*). These differences predominantly result from the different treatment of biogenic particles in the water column. However, simulation *Particle* also contains updates to the Fe cycle which alter export production (Fig. 3c). The simplified Fe scheme employed previously in the Bern3d model results in too much Fe in the surface of the Southern Ocean (see SI), and therefore features a high export production in the pre-industrial Southern Ocean with virtually no Fe limitation. The overestimation of export production in the pre-industrial Southern Ocean causes an overestimation of the export production loss in response to sea ice expansion in the 'cold' simulation.

https://doi.org/10.5194/egusphere-2026-275
Preprint. Discussion started: 16 February 2026

With the updated Fe scheme, the model better represents Fe limitation in the Southern Ocean in the pre-industrial steady state (see the tuning in the SI). Therefore, the model setup *Particle* with the updated Fe cycling shows a smaller reduction in export production in the Southern Ocean in response to cooling than model setup *Particle_oldFe* (Fig. 3c). A smaller reduction in export also means less reduction of overall remineralization in the ocean, and therefore less regenerated DIC decrease (Fig. S2.5; panel d versus f). Instead, the effect of the downward shift of POM remineralization in the Pacific becomes apparent as a slight increase in regenerated DIC (Fig. S2.5f).

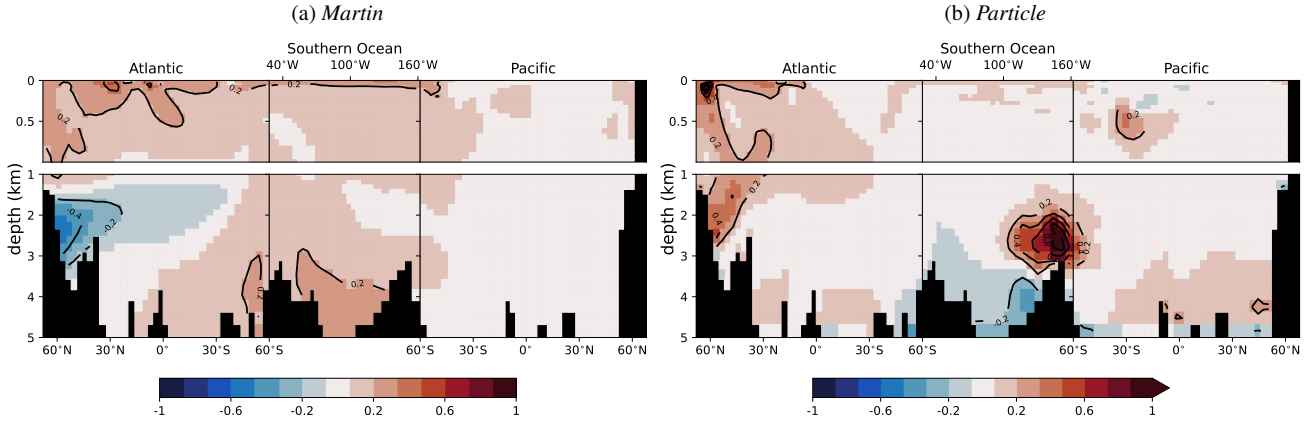

Figure 6. Changes of dissolved Fe concentrations (μmol/m^3) due to the applied cooling in our simulations $Martin_{cold}$ and $Particle_{cold}$ compared to the respective PI state.

The updates to the Fe scheme also alter the response of the Fe distribution to climatic changes, reversing the sign of change in the deep Atlantic and abyssal Southern Ocean (Fig. 6) and add a new feedback from biogenic particle flux changes. In both locations, sedimentary Fe release is reduced due to the reduction of POC reaching the sediments. In extra-polar sediments, Fe release from the sediments mostly increase due to a larger portion of POM reaching the sediments as a consequence of slower remineralization.

Globally integrated, sedimentary Fe release increases slightly in the colder climate state with the updated Fe scheme (Fig. S2.7 and Discussion).

4 Response to warming

https://doi.org/10.5194/egusphere-2026-275
Preprint. Discussion started: 16 February 2026

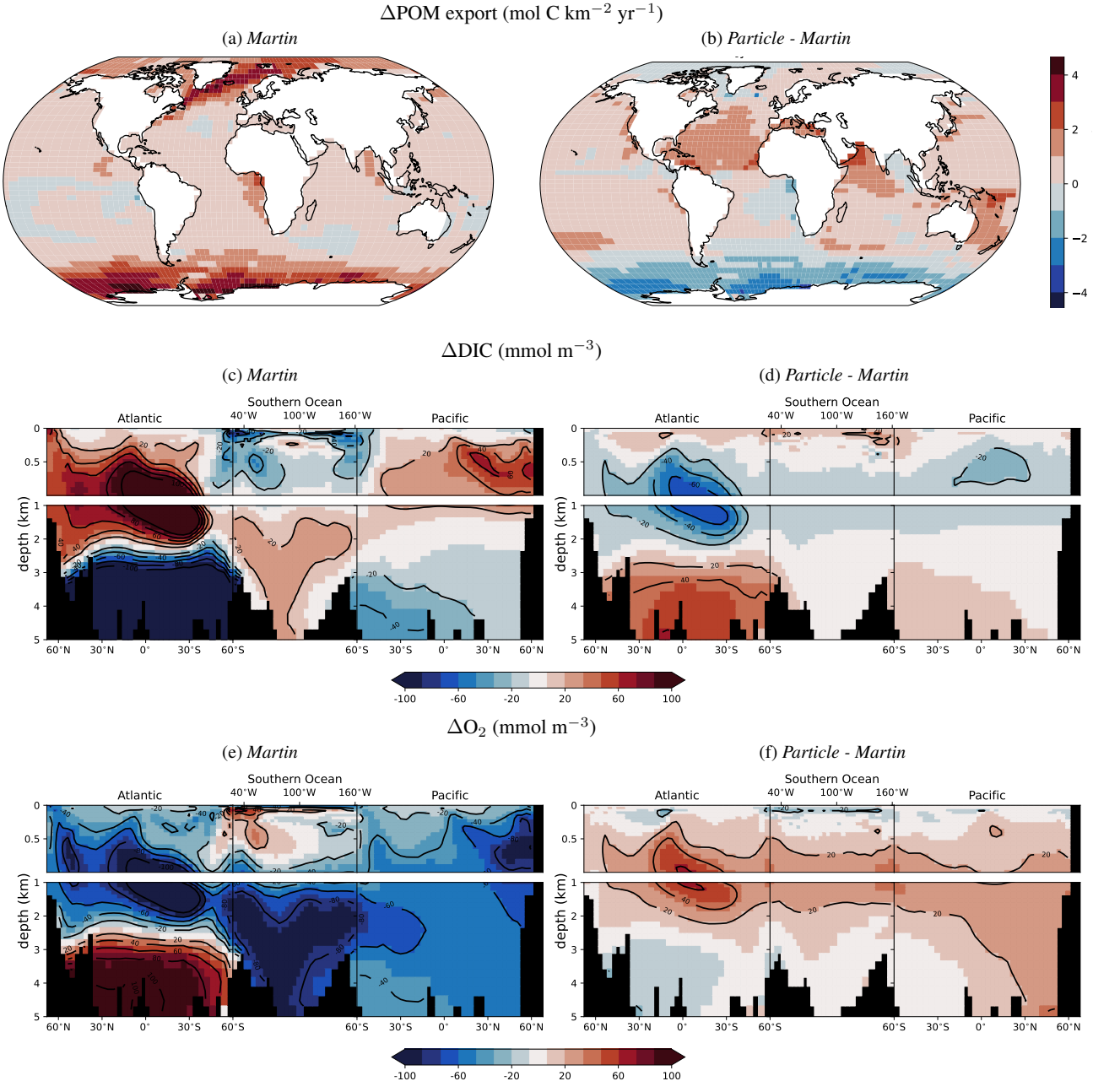

Figure 7. Warming response in POM export, DIC and O_2 in the standard model (a = $Martin_{warm}$ - $Martin_{PI}$, left column) and the effect of the model updates ($Particle_{warm}$ - $Particle_{PI}$ - a, right column).

Like in our simulations of a cold climate state, in our simulation of a warm climate state the dynamic particle fluxes, in combination with the Fe cycle updates, amplify climate-driven global POM export and global DIC changes but in this case

https://doi.org/10.5194/egusphere-2026-275
Preprint. Discussion started: 16 February 2026

dampen global O_2 changes (Table 2). Regionally, the largest export production gains are simulated in sub-polar and polar oceans where previously export-limiting conditions improve due to retreating sea ice and amplified warming (Fig. 7a). The export increase in the North Atlantic emerges in all model setups, while the stronger Fe limitation of export production in the Southern Ocean in *Particle* largely inhibits the productivity gain simulated in *Martin* (Fig. 7b). Instead, temperature-driven increases in shallow remineralization in *Particle* cause more wide-spread increase of export at mid- and low latitudes. The effects of shallower remineralization are also apparent in a global O_2 reduction and DIC increase in the upper water column compared to the *Martin* simulations, accompanied by negative DIC and positive O_2 anomalies between 500 – 1500 m water depth as a consequence of the reduced transfer efficiency (Fig. S2.6).

5 Discussion

The new dynamical particle flux implementation causes a different response of marine biogeochemistry to climate shifts compared to the previous simplified implementation in the Bern3D model. Here, we evaluate whether these differences improve the skill of the model to simulate the Earth system response to climatic change by comparing the results of our cooling scenario with reconstructions of biogeochemical differences between the LGM and today, and then use the simulation with prescribed warming to explore how marine carbon cycling might function in a warm ocean. Importantly to note, however, is that our cooling experiment is highly idealized and is not accounting for a range of additional changes in boundary conditions that occurred over the last 20 000 years.

In the cooling experiment, export production declines in the Southern Ocean and North Atlantic, which is consistent with reconstructions of glacial export production patterns based on agreement between multiple particle flux and degradation proxies (Kohfeld et al., 2005). However, the same reconstruction shows glacial productivity increases north of the polar front in the Southern Ocean, which do not emerge in our simulations. This productivity increase was likely caused by elevated Fe supply from continental dust (Parekh et al., 2008), a response to cooling which is not considered in our idealized experiments. In the equatorial Pacific, the model response is similar to reconstructions indicating reduced productivity in response to cooling (Costa et al., 2016, 2017). Previous studies suggest that the productivity changes in the equatorial Pacific were likely the result of changes in upwelling of nutrients (Doering et al., 2016; Costa et al., 2017). Under colder conditions, POM remineralization shifts toward greater depths, decreasing rapid nutrient recycling at shallow waters. As a result, nutrient concentrations in upwelling waters increase slightly. However, previous studies showed that glacial changes in winds may have reduced the rate of deep water upwelling in the equatorial Pacific (Costa et al., 2017) and that the reconstructed productivity increase in the Southern Ocean could also have reduced nutrient availability in the equatorial Pacific (Costa et al., 2017). This suggest that for realistic paleo-simulation additional wind and dust forcings are key for realistic representations of past conditions on regional scale.

At high latitudes, Liu et al. (2024) simulated faster particle sinking due to ballasting effects by dust particles which we did not simulate here. Instead, similar to the findings by Liu et al. (2024), in our simulations increased preservation of POM in the

https://doi.org/10.5194/egusphere-2026-275
Preprint. Discussion started: 16 February 2026

water column in low and mid-latitudes increases the portion of POM in the composition of sinking particles which reduces the average density of the sinking particle mix and thus their sinking speed.

In all model setups, the cooling causes a DIC increase in the deep Atlantic primarily because of the substantial AMOC weakening (similar to the findings from Liu et al., 2024). In the Pacific, it was suggested based on reconstructed $\delta^{13}C$ and nutrient patterns that regenerated DIC was lower in the upper and higher in the lower water column at the LGM (Sarnthein et al., 2013; Oppo et al., 2018; Peterson and Lisiecki, 2018), which is only simulated with the revised implementation when the temperature dependence in the new dynamic particle flux module shifts remineralization to deeper depths and when export production losses are lower due to the improved Fe scheme (Fig. S2.5).

Concerning the Fe cycling response to the cold climate state, we find an elevated Fe source from sediments, which is opposite to the trend found by Muglia et al. (2017) in their simulations with full LGM boundary conditions. The reasons for their decrease in Fe source are the lowered sea level and the temperature dependency of sedimentary organic matter degradation. Both processes are not included here, since sea level remains constant and we used the parameterisation of sedimentary organic matter oxidation from Dale et al. (2015), which is only a function of the organic matter flux to the sediments. In our simulations, the sedimentary oxidation rate increases due to increased supply of organic matter to sediments, which increases Fe release in addition to reduced oxygenation of benthic waters. These controls on the Fe source dominate also in a simulation in which we explicitly calculate sedimentary oxygenation rates based on organic matter content in the sediments and pore water temperature and oxygen (Fig. S2.7). In both cases, the sedimentary Fe source is increased in a colder climate, and the difference is larger in our simulation with explicit pore water condition changes. In a colder climate, the effects of altered export production, particle remineralization, and sedimentary Fe release combine to reduce Fe limitation on export production in the Atlantic and Southern Ocean, even without any changes to the Fe input from dust deposition. Yet, the result may differ when the effect of lower sea level stand is considered, highlighting the need to discuss changes of Fe cycling beyond aeolian dust inputs to understand nutrient limitation in a glacial ocean.

Overall, the addition of particle dynamics and updates to the Fe scheme improve the agreement of our model results with reconstructed differences in export production and DIC between a colder climate, e.g. the LGM and the Holocene. However, additional forcings and changes in boundary conditions, not considered in these idealized experiments, are required to capture the full Earth system response to such climate change. Changes in ice sheets and albedo, aeolian dust and iron deposition, sea level change, or effects of changes in weathering are not represented in the simulation setup. The energy balance module of Bern3D does also not simulate any changes in winds and their effect on air-sea gas transfer and wind stress. These limitations also apply to our experiments of idealized warming.

In the warming experiment, our model produces at steady-state a net increase of export production, which is further amplified by considering particle flux dynamics. This is in line with other simulations of the steady state response to warming (e.g. Battaglia and Joos, 2018b; Pillot et al., 2025) which show higher or equal export production in warm Earth system states compared to pre-industrial conditions. This is also suggested by proxy data of past warm periods (e.g. Ma et al., 2014; Lyle and Olivarez Lyle, 2024) and marks an important difference between the transient and long-term responses, as in the latter the ocean has fully equilibrated to the warmer climate, with a more vigorous overturning circulation and less nutrient storage in the deep

https://doi.org/10.5194/egusphere-2026-275
Preprint. Discussion started: 16 February 2026

ocean. Temperature-dependent POM remineralization increases the rate of nutrient recycling in the upper water column, which largely increases productivity in our study. This is consistent with other modelling work (Crichton et al., 2021). Like in previous studies with Bern3D, marine oxygen concentrations decrease in our steady state warming simulations as solubility changes and increased export production overcompensate the effect of improved ventilation due to a stronger overturning circulation (Battaglia and Joos, 2018a). Our simulations do not capture the effects of changed marine nitrogen cycling, which has been suggested to reduce marine oxygen usage under long-term warming, hence resulting in a net oxygen concentration increase in a warmer ocean (Oschlies et al., 2019). Particle dynamics in the new model version reduce the oxygen loss in the warmer ocean by one third despite the stronger increase in export production, because warming shifts the mean depth of remineralization in the water column upwards. Warming also reduces the DIC content of the ocean and the dynamic particle scheme amplifies this carbon storage decrease, similar to the findings of other modeling studies (e.g. Segschneider and Bendtsen, 2013). A decreased carbon storage in a warmer ocean is consistent with other steady state simulations of warming (Kleinen et al., 2016; Kessler et al., 2018) but unlike simulations of near-future marine carbon storage changes in which anthropogenic C emissions drive C uptake by the ocean on a larger scale than the warming-driven degassing (Kwiatkowski et al., 2020).

6 Conclusion

The dynamics and environmental controls on biogenic particle remineralization rates are still poorly understood and subjects of ongoing investigation. We updated the Bern3D model to include a representation of the advances in understanding of biogenic particle fluxes in the water column and marine Fe cycling. These new parameterizations clearly improved the model-data comparison for the modern ocean and captures more features of the reconstructed export production differences in a cold Earth system state. With the added complexity, we also introduced new feedbacks that alter the simulated response of biogeochemical cycling in the ocean to different background climates. In particular, environmental controls on organic particle remineralization and carbonate dissolution alter the accumulation of regenerated and preformed DIC in the deep ocean, resulting in an overall increased marine carbon storage and reduced oxygenation in a colder ocean. In our simulation of a warmer steady-state ocean, particle dynamics amplify the increases in export production and marine carbon losses that are simulated with the simplified Martin curve scheme, but reduce the simulated O_2 loss. This highlights the necessity to better understand and model the complexity of marine production and carbon cycling for robust projections of the future marine carbon sink and marine deoxygenation.

Code and data availability. The simulation results and the source code of the particle flux and Fe cycle modules are available online (Adloff et al., 2026).

Competing interests. The authors declare no competing interests.

https://doi.org/10.5194/egusphere-2026-275
Preprint. Discussion started: 16 February 2026

F.J., A.D. and C.L. conceptualized the implementation of MSPACMAM in Bern3D. M.A. and F.P. did the programming. M.A. tuned the model, produced the simulations and produced the figures. All authors discussed the results and wrote the manuscript.

Acknowledgements. M.A. and F.J. acknowledge support by Swiss National Science Foundation under grant 200020_200511. C.L. acknowledges support from the Swiss National Science Foundation under grant 203448. F.P. is funded by the European Union's Horizon Europe research and innovation program under Grant Agreement No. 101184070 (Past-To-Future).

https://doi.org/10.5194/egusphere-2026-275
Preprint. Discussion started: 16 February 2026

References

Adloff, M., Jeltsch-Thömmes, A., Pöppelmeier, F., Stocker, T. F., and Joos, F. (2025). Sediment fluxes dominate glacial–interglacial changes in ocean carbon inventory: results from factorial simulations over the past 780 000 years. *Climate of the Past*, 21(2):571–592.

Adloff, M., Pöppelmeier, F., Dinauer, A., Laufkötter, C., and Joos, F. (2026). Publication resources. *Dataset*.

Armstrong, R. A., Lee, C., Hedges, J. I., Honjo, S., and Wakeham, S. G. (2001). A new, mechanistic model for organic carbon fluxes in the ocean based on the quantitative association of POC with ballast minerals. *Deep Sea Research Part II: Topical Studies in Oceanography*, 49(1-3):219–236.

Armstrong, R. A., Peterson, M. L., Lee, C., and Wakeham, S. G. (2009). Settling velocity spectra and the ballast ratio hypothesis. *Deep Sea Research Part II: Topical Studies in Oceanography*, 56(18):1470–1478.

Battaglia, G. and Joos, F. (2018a). Hazards of decreasing marine oxygen: the near-term and millennial-scale benefits of meeting the Paris climate targets. *Earth system dynamics*, 9(2):797–816.

Battaglia, G. and Joos, F. (2018b). Marine N_2O emissions from nitrification and denitrification constrained by modern observations and projected in multimillennial global warming simulations. *Global Biogeochemical Cycles*, 32(1):92–121.

Bendtsen, J., Lundsgaard, C., Middelboe, M., and Archer, D. (2002). Influence of bacterial uptake on deep-ocean dissolved organic carbon. *Global Biogeochemical Cycles*, 16(4):74–1.

Buchanan, P. J., Matear, R. J., Lenton, A., Phipps, S. J., Chase, Z., and Etheridge, D. M. (2016). The simulated climate of the last glacial maximum and insights into the global marine carbon cycle. *Climate of the Past*, 12(12):2271–2295.

Cliff, E., Khatiwala, S., and Schmittner, A. (2021). Glacial deep ocean deoxygenation driven by biologically mediated air–sea disequilibrium. *Nature Geoscience*, 14(1):43–50.

Costa, K. M., Jacobel, A. W., McManus, J. F., Anderson, R. F., Winckler, G., and Thiagarajan, N. (2017). Productivity patterns in the equatorial pacific over the last 30,000 years. *Global Biogeochemical Cycles*, 31(5):850–865.

Costa, K. M., McManus, J. F., Anderson, R. F., Ren, H., Sigman, D. M., Winckler, G., Fleisher, M. Q., Marcantonio, F., and Ravelo, A. C. (2016). No iron fertilization in the equatorial pacific ocean during the last ice age. *Nature*, 529(7587):519–522.

Crichton, K. A., Wilson, J. D., Ridgwell, A., and Pearson, P. N. (2021). Calibration of temperature-dependent ocean microbial processes in the cgenie. muffin (v0. 9.13) earth system model. *Geoscientific Model Development*, 14(1):125–149.

Dale, A. W., Nickelsen, L., Scholz, F., Hensen, C., Oschlies, A., and Wallmann, K. (2015). A revised global estimate of dissolved iron fluxes from marine sediments. *Global Biogeochemical Cycles*, 29(5):691–707.

Deutsch, C., Sigman, D. M., Thunell, R. C., Meckler, A. N., and Haug, G. H. (2004). Isotopic constraints on glacial/interglacial changes in the oceanic nitrogen budget. *Global Biogeochemical Cycles*, 18(4).

Dinauer, A., Laufkötter, C., Doney, S. C., and Joos, F. (2022). What controls the large-scale efficiency of carbon transfer through the ocean's mesopelagic zone? insights from a new, mechanistic model (mspacmam). *Global biogeochemical cycles*, 36(10):e2021GB007131.

Doering, K., Erdem, Z., Ehlert, C., Fleury, S., Frank, M., and Schneider, R. (2016). Changes in diatom productivity and upwelling intensity off peru since the last glacial maximum: Response to basin-scale atmospheric and oceanic forcing. *Paleoceanography*, 31(10):1453–1473.

Doney, S. C., Lindsay, K., Fung, I., and John, J. (2006). Natural variability in a stable, 1000-yr global coupled climate–carbon cycle simulation. *Journal of climate*, 19(13):3033–3054.

Edwards, N. R., Willmott, A. J., and Killworth, P. D. (1998). On the role of topography and wind stress on the stability of the thermohaline circulation. *J PHYS OCEANOGR*, 28(5):756–778.

https://doi.org/10.5194/egusphere-2026-275
Preprint. Discussion started: 16 February 2026

Galbraith, E. D. and Skinner, L. C. (2020). The biological pump during the last glacial maximum. *Annual Review of Marine Science*, 12:559–586.

Griffies, S. M. (1998). The Gent–McWilliams skew flux. *J PHYS OCEANOGR*, 28(5):831–841.

Hülse, D., Arndt, S., Wilson, J. D., Munhoven, G., and Ridgwell, A. (2017). Understanding the causes and consequences of past marine carbon cycling variability through models. *Earth-Science Reviews*, 171:349–382.

Jeltsch-Thömmes, A., Battaglia, G., Cartapanis, O., Jaccard, S. L., and Joos, F. (2019). Low terrestrial carbon storage at the last glacial maximum: constraints from multi-proxy data. *Climate of the Past*, 15(2):849–879.

Kessler, A., Galaasen, E. V., Ninnemann, U. S., and Tjiputra, J. (2018). Ocean carbon inventory under warmer climate conditions–the case of the last interglacial. *Climate of the Past*, 14(12):1961–1976.

Kleinen, T., Brovkin, V., and Munhoven, G. (2016). Modelled interglacial carbon cycle dynamics during the holocene, the eemian and marine isotope stage (mis) 11. *Climate of the Past*, 12(12):2145–2160.

Kohfeld, K. E., Quere, C. L., Harrison, S. P., and Anderson, R. F. (2005). Role of marine biology in glacial-interglacial co2 cycles. *Science*, 308(5718):74–78.

Kwiatkowski, L., Torres, O., Bopp, L., Aumont, O., Chamberlain, M., Christian, J. R., Dunne, J. P., Gehlen, M., Ilyina, T., John, J. G., et al. (2020). Twenty-first century ocean warming, acidification, deoxygenation, and upper-ocean nutrient and primary production decline from CMIP6 model projections. *Biogeosciences*, 17(13):3439–3470.

Kwon, E. Y., Primeau, F., and Sarmiento, J. L. (2009). The impact of remineralization depth on the air–sea carbon balance. *Nature Geoscience*, 2(9):630–635.

Laufkötter, C., John, J. G., Stock, C. A., and Dunne, J. P. (2017). Temperature and oxygen dependence of the remineralization of organic matter. *Global Biogeochemical Cycles*, 31(7):1038–1050.

Liang, H., Lunstrum, A. M., Dong, S., Berelson, W. M., and John, S. G. (2023). Constraining $caco_3$ export and dissolution with an ocean alkalinity inverse model. *Global Biogeochemical Cycles*, 37(2):e2022GB007535.

Liu, B., Maerz, J., and Ilyina, T. (2024). Glacial atlantic carbon storage enhanced by a shallow amoc and marine aggregates sinking. *Geophysical Research Letters*, 51(24):e2024GL109736.

Lyle, M. and Olivarez Lyle, A. (2024). Variations in the Biological Pump through the Miocene: Evidence from organic carbon burial in Pacific Ocean sediments. *Climate of the Past Discussions*, 2024:1–20.

Ma, Z., Gray, E., Thomas, E., Murphy, B., Zachos, J., and Paytan, A. (2014). Carbon sequestration during the palaeocene–eocene thermal maximum by an efficient biological pump. *Nature Geoscience*, 7(5):382–388.

Mahowald, N. M., Muhs, D. R., Levis, S., Rasch, P. J., Yoshioka, M., Zender, C. S., and Luo, C. (2006). Change in atmospheric mineral aerosols in response to climate: Last glacial period, preindustrial, modern, and doubled carbon dioxide climates. *Journal of Geophysical Research: Atmospheres*, 111(D10).

Martin, J. H. (1990). Glacial-interglacial CO_2 change: The iron hypothesis. *Paleoceanography*, 5(1):1–13.

Matsumoto, K. (2007). Biology-mediated temperature control on atmospheric pco_2 and ocean biogeochemistry. *Geophysical Research Letters*, 34(20).

Matsumoto, K., Hashioka, T., and Yamanaka, Y. (2007). Effect of temperature-dependent organic carbon decay on atmospheric pco_2. *Journal of Geophysical Research: Biogeosciences*, 112(G2).

Muglia, J., Somes, C. J., Nickelsen, L., and Schmittner, A. (2017). Combined effects of atmospheric and seafloor iron fluxes to the glacial ocean. *Paleoceanography*, 32(11):1204–1218.

https://doi.org/10.5194/egusphere-2026-275
Preprint. Discussion started: 16 February 2026

Müller, S., Joos, F., Edwards, N., and Stocker, T. (2006). Water mass distribution and ventilation time scales in a cost-efficient, three-dimensional ocean model. *J CLIMATE*, 19(21):5479–5499.

Nickelsen, L., Keller, D., and Oschlies, A. (2015). A dynamic marine iron cycle module coupled to the University of Victoria Earth System Model: the Kiel Marine Biogeochemical Model 2 (KMBM2) for UVic.

Oppo, D. W., Gebbie, G., Huang, K.-F., Curry, W. B., Marchitto, T. M., and Pietro, K. R. (2018). Data constraints on glacial atlantic water mass geometry and properties. *Paleoceanography and Paleoclimatology*, 33(9):1013–1034.

Oschlies, A., Koeve, W., Landolfi, A., and Kähler, P. (2019). Loss of fixed nitrogen causes net oxygen gain in a warmer future ocean. *Nature Communications*, 10(1):2805.

Parekh, P., Follows, M. J., and Boyle, E. (2004). Modeling the global ocean iron cycle. *Global biogeochemical cycles*, 18(1).

Parekh, P., Joos, F., and Müller, S. A. (2008). A modeling assessment of the interplay between aeolian iron fluxes and iron-binding ligands in controlling carbon dioxide fluctuations during antarctic warm events. *Paleoceanography*, 23(4).

Peterson, C. D. and Lisiecki, L. E. (2018). Deglacial carbon cycle changes observed in a compilation of 127 benthic δ^{13}C time series (20–6 ka). *Climate of the Past*, 14(8):1229–1252.

Pillot, Q., Sarr, A.-C., Donnadieu, Y., Gramoullé, A., and Suchéras-Marx, B. (2025). Impact of dust and temperature on primary productivity in late miocene oceans. *Paleoceanography and Paleoclimatology*, 40(1):e2023PA004838.

Poletti, A., Frierson, D., and Armour, K. (2024). Why do co2 quadrupling simulations warm more than twice as much as co2 doubling simulations in cmip6? *Geophysical Research Letters*, 51(10):e2023GL107320.

Pöppelmeier, F., Joos, F., and Stocker, T. F. (2023). The Coupled Ice Sheet–Earth System Model Bern3D v3. 0. *Journal of Climate*, 36(21):7563–7582.

Roth, R., Ritz, S., and Joos, F. (2014). Burial-nutrient feedbacks amplify the sensitivity of atmospheric carbon dioxide to changes in organic matter remineralisation. *Earth System Dynamics*, 5(2):321–343.

Sarnthein, M., Schneider, B., and Grootes, P. M. (2013). Peak glacial ^{14}C ventilation ages suggest major draw-down of carbon into the abyssal ocean. *Climate of the Past*, 9(6):2595–2614.

Segschneider, J. and Bendtsen, J. (2013). Temperature-dependent remineralization in a warming ocean increases surface pco_2 through changes in marine ecosystem composition. *Global Biogeochemical Cycles*, 27(4):1214–1225.

Smith, C. J., Kramer, R. J., Myhre, G., Alterskjær, K., Collins, W., Sima, A., Boucher, O., Dufresne, J.-L., Nabat, P., Michou, M., et al. (2020). Effective radiative forcing and adjustments in cmip6 models. *Atmospheric Chemistry and Physics*, 20(16):9591–9618.

Somes, C. J., Dale, A. W., Wallmann, K., Scholz, F., Yao, W., Oschlies, A., Muglia, J., Schmittner, A., and Achterberg, E. P. (2021). Constraining Global Marine Iron Sources and Ligand-Mediated Scavenging Fluxes With GEOTRACES Dissolved Iron Measurements in an Ocean Biogeochemical Model. *Global Biogeochemical Cycles*, 35(8):e2021GB006948.

St. Laurent, L., Simmons, H., and Jayne, S. (2002). Estimating tidally driven mixing in the deep ocean. *Geophysical research letters*, 29(23):21–1.

Tagliabue, A., Buck, K. N., Sofen, L. E., Twining, B. S., Aumont, O., Boyd, P. W., Caprara, S., Homoky, W. B., Johnson, R., König, D., et al. (2023). Authigenic mineral phases as a driver of the upper-ocean iron cycle. *Nature*, 620(7972):104–109.

Taucher, J., Bach, L. T., Riebesell, U., and Oschlies, A. (2014). The viscosity effect on marine particle flux: A climate relevant feedback mechanism. *Global Biogeochemical Cycles*, 28(4):415–422.

Tierney, J. E., Zhu, J., King, J., Malevich, S. B., Hakim, G. J., and Poulsen, C. J. (2020). Glacial cooling and climate sensitivity revisited. *Nature*, 584(7822):569–573.

https://doi.org/10.5194/egusphere-2026-275
Preprint. Discussion started: 16 February 2026

Tschumi, T., Joos, F., and Parekh, P. (2008). How important are Southern Hemisphere wind changes for low glacial carbon dioxide? A model study. *PALEOCEANOGRAPHY*, 23(4).

Volk, T. and Hoffert, M. I. (1985). Ocean carbon pumps: Analysis of relative strengths and efficiencies in ocean-driven atmospheric CO_2 changes. *The carbon cycle and atmospheric CO2: Natural variations Archean to present*, 32:99–110.